

Path sampling challenges in large biomolecular systems: RETIS and REPPTIS for ABL-imatinib kinetics

Wouter Vervust¹, Daniel T. Zhang², Enrico Riccardi³, Titus S. van Erp⁴, and An Ghysels^{1,*}

¹IBiTech - BioMMedA research group, Ghent University, Corneel Heymanslaan 10, entrance 97, 9000 Gent, Belgium

²Research Institute for Interdisciplinary Science, Okayama University, Okayama 700-8530, Japan

³Department of Energy Resources, University of Stavanger, Stavanger, Norway

⁴Department of Chemistry, Norwegian University of Science and Technology, NO-7491 Trondheim, Norway

*Correspondence: an.ghysels@ugent.be

ABSTRACT

Predicting the kinetics of drug-protein interactions is crucial for understanding drug efficacy, particularly in personalized medicine, where protein mutations can significantly alter drug residence times. This study applies Replica Exchange Transition Interface Sampling (RETIS) and its Partial Path variant (REPPTIS) to investigate the dissociation kinetics of imatinib from Abelson nonreceptor tyrosine kinase (ABL) and mutants relevant to chronic myeloid leukemia therapy. These path-sampling methods offer a bias-free alternative to conventional approaches requiring qualitative predefined reaction coordinates. Nevertheless, the complex free-energy landscape of ABL-imatinib dissociation presents significant challenges. Multiple metastable states and orthogonal barriers lead to parallel unbinding pathways, complicating convergence in TIS-based methods. Despite employing computational efficiency strategies such as asynchronous replica exchange, full convergence remained elusive. This work provides a critical assessment of path sampling in high-dimensional biological systems, discussing the need for enhanced initialization strategies, advanced Monte Carlo path generation moves, and machine learning-derived reaction coordinates to improve kinetic predictions of drug dissociation with minimal prior knowledge.

SIGNIFICANCE This study examines the dissociation kinetics of imatinib from ABL kinase using RETIS and REPPTIS, assessing the feasibility of path sampling methods for drug unbinding in a clinically relevant system. ABL mutations drive imatinib resistance in chronic myeloid leukemia, underscoring the need for computational tools that predict mutation-induced kinetic effects. However, the complex energy landscape, metastable states, and parallel unbinding pathways posed significant challenges, revealing limitations of one-dimensional reaction coordinates. This work highlights the need for improved initialization strategies and higher-dimensional approaches to enhance the predictive power of path sampling in biomolecular kinetics, providing insights that guide future advancements in computational drug design and personalized medicine.

INTRODUCTION

Traditionally, equilibrium thermodynamic properties such as binding affinity (dissociation constant K_d) and IC_{50} (concentration causing 50% target inhibition) have dominated as primary predictors of drug efficacy (1–4). However, drug kinetics, particularly drug residence time, has been increasingly recognized for its crucial role in pharmacodynamics and better correlation with *in vivo* efficacy (5–9).

Personalized medicine is particularly relevant for kinase inhibitors, where protein mutations can drastically alter drug residence times, affecting therapeutic effectiveness (10–12). A well-known example is Abelson nonreceptor tyrosine kinase (ABL), which plays a significant role in chronic

myeloid leukemia (CML) through its fusion oncogene BCR-ABL (13, 14). The first-generation tyrosine kinase inhibitor (TKI) imatinib (Gleevec[®], also known as STI571) was developed to competitively bind to the ATP-binding site. Imatinib demonstrated remarkable efficacy in the treatment of CML and is recognized as a landmark achievement in targeted drug design (13–15). However, mutations in the ABL kinase domain led to resistance, necessitating the development of second- and third-generation TKIs (14, 16). This iterative arms race between targeted therapy and resistance mutations underscores the necessity of predictive tools that assess how mutations drive changes in drug kinetics.

Given the costly and time-consuming nature of experi-

mental residence time assays, computational methods have emerged as a promising alternative in the early stages of the drug-design pipeline (5, 17–20). Molecular dynamics (MD) simulations can provide valuable insight into the mechanisms of drug unbinding and even provide a timescale on drug dissociation. The unbinding mechanism is, however, often a rare event, where dissociation is preceded by a long waiting time – in terms of computer simulation wall time. Moreover, multiple occurrences need to be observed to obtain reasonable statistics. Even with the current high performance computing infrastructure, this prevents the application of standard MD simulations to assess and predict timescales of biological processes that occur less frequently than several times per 10 μ s. For instance, predicting a drug residence time of 1 ms lies beyond what is currently feasible.

To overcome this, path sampling methodologies have been developed to efficiently explore rare events by focusing computational effort on transition events rather than waiting times (21–23). Several methods have been developed based on path ensembles (24), including transition interface sampling (TIS) (25), which gives exact kinetics (26). Milestoning (27, 28) and the partial path variant of TIS (PPTIS) (29) introduce a Markovian approximation, statistically combining short trajectory segments to reconstruct the full transition efficiently, especially for rare and long transitions. The efficiency of the exact TIS methods can be enhanced by incorporating swaps between ensembles, as implemented in replica exchange TIS (RETIS) (30–32), in its partial path counterpart called replica exchange PPTIS (REPPTIS) (33), and in the recently developed infinite swap and asynchronous version called ∞ RETIS (34). (RE)TIS methods have been successfully applied to study chemical reactions (35–37), thin film breakage (38, 39), solid-solid phase transitions in crystal structures (40), protein-DNA interaction (41) and permeation of oxygen through membranes (42, 43). However, their applicability to large biological systems, such as kinase-drug dissociation, remains largely untested.

In this work, we explore the application of RETIS, REPTIS, and ∞ RETIS to imatinib dissociation from wild-type and mutant ABL kinase domains, assessing the feasibility of these methods for studying mutation-driven effects on drug kinetics. Imatinib dissociation from ABL is found to be characterized by the presence of metastable states and multiple parallel dissociation pathways, which introduce significant challenges for the current TIS-based sampling methodologies, including sampling bottlenecks, slow convergence, and difficulties in defining optimal reaction coordinates. Our paper highlights these key computational challenges and offers an outlook on necessary methodological developments to improve the predictive capabilities of RE(PP)TIS for drug dissociation kinetics.

The remainder of this work is structured as follows. In the [Methods](#), the ABL-imatinib complex is briefly described, followed by a description of the (RE)(PP)TIS methodologies. The equilibrium simulations, the order parameter definitions,

and the steered simulations that are required to initialize the path sampling simulations are then discussed. The section ends with optimizations that were implemented to speed up the path sampling simulations. The [Results](#) show how metastable states and parallel distinct reaction channels characterize imatinib dissociation, and it is discussed how these two factors limit the current RE(PP)TIS methodology in the [Discussion](#). The [Future Perspectives and Conclusion](#) then give an outlook on how to tackle these challenges.

METHODS

The ABL-imatinib complex

The ABL kinase domain is shown in Fig. 1, consisting of the N-terminal and C-terminal lobes typical for protein kinases. Three important regions are highlighted: the activation loop (A-loop, red), the ATP-binding loop (P-loop, green), and the α C-helix (magenta). The N-lobe consists of a five stranded β -sheet and the α C-helix, and also contains the P-loop. The C-lobe mainly consists of helical structures and contains the substrate binding site (44). The active site (ATP-binding site) is located in the cleft between the N- and C-lobes.

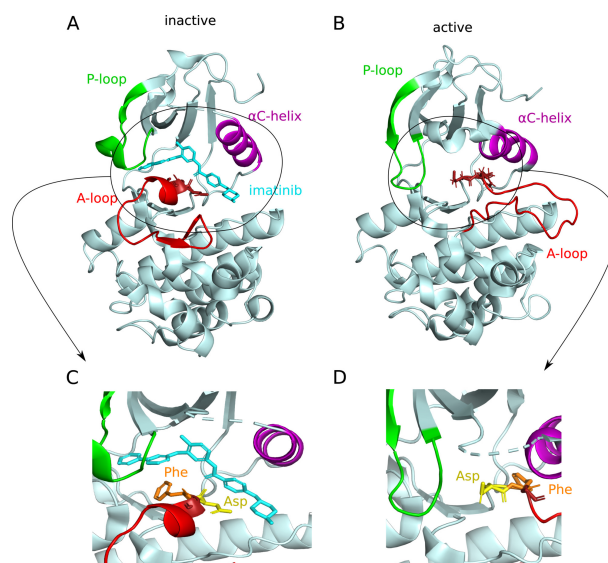


Figure 1: Inactive (A, PDB 6NPV (45)) and active (B, PDB 6XR6 (46)) conformations of the ABL kinase domain. C: Close up of the binding pocket in the inactive state. Imatinib binds to the inactive state, where the aspartate residue points outwards of the binding pocket. D: Close up of the binding pocket in the active state. In the active state, the aspartate residue points inwards of the binding pocket. In A and B, the dashed cyan lines represent missing residues of the 6NPV structure. In D, the dashed cyan lines represent removed residues for better visualization of the binding pocket. Figure created with PyMOL (47).

Located at the N-terminal side of the A-loop is the aspartate-phenylalanine-glycine (DFG) motif. The active state

is characterized by the aspartate pointing inwards towards the ATP-binding site (DFG-in, Fig. 1D). Transitioning to the inactive state is accompanied by the DFG motif flipping 180°, where the aspartate residue moves outwards and the phenylalanine moves inwards (DFG-out, Fig. 1C) (44). In the active state, the α C-helix is turned away from the hinge region, and the A-loop is in an open (extended) conformation. In the inactive state, the α C-helix is turned towards the hinge region, and the A-loop can block substrate binding to the C-lobe.

The ABL kinase domain catalyzes the transfer of the γ -phosphate from adenosine triphosphate (ATP) to tyrosine residues in substrate proteins (44). Patients with the fusion oncogene BCR-ABL suffer from chronic myeloid leukemia (CML), where the normally autoinhibited kinase domain becomes constitutively active (13, 14). Imatinib inhibits this activity by competitively binding to the ATP-binding site, thereby preventing ATP from engaging with the kinase. However, ABL mutations can confer resistance by destabilizing imatinib binding or favoring conformations that reduce drug affinity (48, 49). To computationally assess how such mutations influence imatinib residence time, REPPTIS and ∞ RETIS are used to investigate imatinib dissociation in both the wild-type (WT) ABL kinase and seven commonly encountered mutated variants for which experimental dissociation constants are available (Table 1).

| Variant | H ₂ O | Na ⁺ | Cl ⁻ |
|---------|------------------|-----------------|-----------------|
| WT | 17355 | 61 | 53 |
| Q252H | 17359 | 61 | 53 |
| Y253F | 17360 | 61 | 53 |
| E255V | 17362 | 60 | 53 |
| T315I | 18858 | 62 | 56 |
| M351T | 17358 | 61 | 53 |
| F359V | 17364 | 61 | 53 |
| H396P | 17358 | 61 | 53 |

Table 1: The ABL-imatinib variants studied in this work. WT denotes the wild-type ABL kinase. The columns specify the number of H₂O molecules, Na⁺ ions, and Cl⁻ ions used in the MD simulation boxes. Variants were selected based on whether PBD structures and experimental dissociation constants (K_D) with imatinib were available, after which seven were selected at different residue index positions.

RETIS and REPPTIS theory

A brief overview of the TIS and PPTIS methodologies, including the (infinite) replica exchange formalism, is now given. Additional information is provided in Text S1, while in-depth discussions can be found in Refs. (29, 32–34, 50). In both TIS and PPTIS, an order parameter λ is defined to track the progression of the reaction, along which $n+1$ non-intersecting hypersurfaces (interfaces) $\{x|\lambda(x) = \lambda_i\}, \forall i \in \{0, \dots, n\}$ are defined (Fig. S1), where x denotes the phase point of the sys-

tem. The interfaces are monotonically increasing ($\lambda_i < \lambda_{i+1}$), where the region left of $\lambda_0 \equiv \lambda_A$ defines state A (A is $\{x|\lambda(x) < \lambda_A\}$) and the region right of $\lambda_n \equiv \lambda_B$ defines state B (B is $\{x|\lambda(x) > \lambda_B\}$).

To each interface λ_i , a path ensemble $[i^+]$ (TIS, Fig. S1B) or $[i^\pm]$ (PPTIS, Fig. S1C) is associated. For TIS, the $[i^+]$ ensemble consists of all the paths that start at λ_A , then cross λ_i before recrossing λ_A , and end in either λ_B or λ_A . For PPTIS, the paths of $[i^\pm]$ are also required to cross λ_i , but the starting and ending conditions are set at the neighboring interfaces λ_{i-1} and λ_{i+1} , meaning that the paths are cut short. For both TIS and PPTIS, the ensemble associated to λ_i allows the calculation of a (conditional) local crossing probability, which is the chance that a path that has just crossed λ_i will cross the next interface λ_{i+1} rather than going back to λ_A (TIS) or λ_{i-1} (PPTIS). For TIS, the crossing behavior around λ_i is thus analyzed using paths that started with escaping A , meaning that all ‘path memory’ is incorporated, resulting in an essentially exact kinetic reconstruction. This reconstruction is done by viewing the rate constant k_{AB} as the product of a positive flux f_A (how many times does the system escape state A , per unit of time) and a global crossing probability $P_A(\lambda_B|\lambda_A)$ (how likely is an escape from state A to result in reaching state B , rather than returning to state A)

$$k_{AB} = f_A \times P_A(\lambda_B|\lambda_A). \quad (1)$$

The flux f_A can be easily computed from a straightforward MD simulation, as in TIS and PPTIS, or, as in RETIS, from the average path lengths in the ensembles $[0^+]$ and the RETIS-specific path ensemble $[0^-]$, which explores the left side of λ_A . The global crossing probability, however, is typically too small to be computed directly. Instead, it is expressed as a product of local conditional crossing probabilities $P_A(\lambda_{i+1}|\lambda_i)$, which represent the probability of reaching λ_{i+1} given that λ_i has been reached. This probability is equivalent to the fraction of sampled paths in $[i^+]$ that cross λ_{i+1} . The number and placement of interfaces are chosen such that $P_A(\lambda_{i+1}|\lambda_i)$ are sufficiently large to be estimated accurately with a relatively modest number of trajectories. In this work, the number of interfaces and their placements for the ABL-imatinib systems were first estimated from a rough free energy calculation using umbrella sampling (US), as shown in Fig. S6.

The catch for TIS lies in the presence of metastable states, where paths can get stuck and commit neither to A nor B , resulting in (computationally) infeasible long paths. For PPTIS, the crossing behavior around λ_i is analyzed using shorter paths whose memory has been cut (Text S1, Fig. S1C), resulting in an essentially approximative reconstruction of the kinetics that is, however, faster and more feasible when barrier-crossing trajectories are not only rare but also very long. The total crossing probability in PPTIS is calculated from recursive relations that use as input the local conditional crossing probabilities p_i^+ , p_i^- , p_i^\mp , and p_i^\ddagger . Here, the top plus or minus sign indicates the probability of transitioning from λ_i

to λ_{i+1} or λ_{i-1} , respectively, while the bottom sign indicates the previous state of the system before crossing λ_i .

Practically, the ensembles [i^+] (TIS) or [i^\pm] (PPTIS) are sampled using a Monte Carlo procedure. New paths are generated from old ones using shooting moves (or more advanced variants (39, 51–56)). A different kind of move is given by replica exchange, where it is attempted to swap paths between different ensembles (Text S1, Fig. S2), resulting in an increase of ergodic sampling and faster convergence for both RETIS and REPPTIS (30, 33). The recently released ∞ RETIS method maximizes the benefits of replica exchange by considering all (infinite) possible swaps after every shooting-like move (39, 57). This approach is particularly suited for parallel computing, where replica exchange moves can be executed asynchronously. Achieving the infinite swapping limit at each step enhances sampling efficiency, making ∞ RETIS a highly efficient method for advanced molecular simulations (34, 57).

Application of RE(PP)TIS to the ABL-imatinib variants requires the definition of an order parameter and the construction of initial paths to which the MC moves can be applied. The initial paths are constructed using steered MD simulations preceded by equilibrium simulations, which are detailed in the following sections.

Equilibrium simulations

The crystal structure of the ABL kinase domain in complex with imatinib was obtained from the 6NPV PDB entry (45). As there were no structures available for 6 of the 7 mutated ABL variants in complex with imatinib or similar TKIs, CHARMM-GUI (58) was used to mutate the residues based on the 6NPV structure. For the gatekeeper mutation T315I, a crystal structure was available in complex with the inhibitor DCC-2036 (PDB entry 3QRJ (59)). To create the T315I variant, the 3QRJ structure was superimposed on the 6NPV structure, the DCC-2036 ligand was removed, and the imatinib ligand added, as shown in Fig. S4.

The structures were then prepared for MD simulations using the GROMACS (60) software package (version 2021.3). The CHARMM36m force field (61) was used for the protein and solvent, where the TIP3P water model was used (62). The force field parameters for imatinib were taken from Ref. (63), which were obtained using QM calculations using the GAAMP software (64, 65) and which were recently used in another study on the WT ABL-imatinib complex (66). The ligand force field was provided in CHARMM format, and it was converted to the GROMACS format using CHARMM-GUI (58). The imatinib parameters define a protonated state, which is desirable as at physiological pH the complex with neutral imatinib represents less than 0.1% of the overall population (67).

The structures were solvated in a rhombic dodecahedron box, ensuring a minimum distance of 1.5 nm between periodic images. The dodecahedral box is only 71% of the cubic box volume with the same minimum distance criterion, resulting

in significant computational savings. The minimal image distance is chosen to be larger than the typical 1 nm value as dissociation is to be studied. Na⁺ and Cl⁻ ions were added to neutralize the system and to reach a physiological salt concentration of 0.15 M. The water and ion content of the simulation boxes is shown in Table 1. The systems were then energy minimized using steepest descent until the maximum force was below 1000 kJ mol⁻¹ nm⁻¹. The systems were then equilibrated in the NVT and NPT ensemble for 100 ps, each, where both the ligand and protein heavy atoms were restrained. The equilibrium production simulations (unrestrained) were run for 50 ns each, in the NPT ensemble at 300 K and at 1 bar using the Bussi–Donadio–Parrinello thermostat (68) with a coupling constant of 0.1 ps and the Parinello–Rahman barostat (69) with a coupling constant of 2 ps and compressibility of 4.5e-5 bar⁻¹. Hydrogen bonds were constrained using LINCS (70), which allowed for a time step of 2 fs.

The equilibrium production simulations were checked for validity (temperature, energy, pressure) and by visualizing the trajectories with the VMD (71) software. A set of rigid C_α's was determined for each variant based on the fluctuations in the 50 ns equilibrium MD run (Table S1). The root mean square deviation (RMSD) and root mean square fluctuations (RMSF) of the protein C_α's are shown in Fig. 2, where protein alignment was performed using the rigid C_α's only, and where the first frame served as reference.

Order parameter definition

The order parameter $\lambda(x)$ for a configuration (snapshot, frame) x is defined as the distance between the current center of mass (COM) of imatinib $\mathbf{r}_{\text{COM}}(x)$ and the average bound COM position of imatinib $\mathbf{r}_{\text{COM}}^{\text{bound}}$,

$$\lambda(t) = \|\mathbf{r}_{\text{COM}}(t) - \mathbf{r}_{\text{COM}}^{\text{bound}}\| \quad (2)$$

where $\mathbf{r}_{\text{COM}}^{\text{bound}}$ approximates the natural bound position of imatinib, which is defined as follows. First, for each variant, the frames of the 50 ns equilibrium trajectory were superposed on the final frame of the trajectory using the rigid C_α's (i.e. the reference frame x_{ref} was the final frame). Second, the average COM position of imatinib in the superimposed frames was calculated and defined as $\mathbf{r}_{\text{COM}}^{\text{bound}}$.

The order parameter $\lambda(x(t))$ of a new frame $x(t)$ can now be calculated by first superposing this new frame to the reference frame x_{ref} using the rigid C_α's, after which the current COM position of imatinib $\mathbf{r}_{\text{COM}}(t)$ is calculated, and its distance to $\mathbf{r}_{\text{COM}}^{\text{bound}}$ is calculated (Eq. 2). As an example, the order parameters are calculated for the equilibrium MD trajectories and shown in Fig. 3, where metastable states are seen to be present even in the deep binding pocket of ABL. This is particularly visible for the Q252H variant (Fig. 3A), where the first 12 ns of the trajectory are spent in a metastable state (Fig. S5) that is clearly separated from the remaining 38 ns. It was chosen not to incorporate the initial 12 ns of the

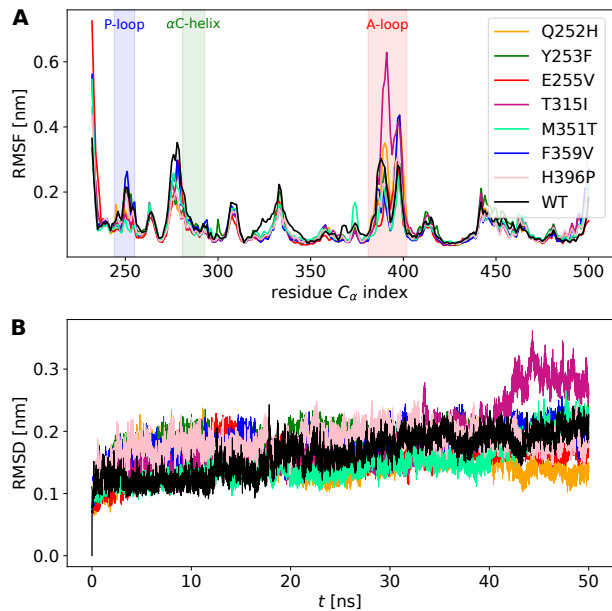


Figure 2: RMSF (A) and RMSD (B) of the C_{α} atoms in equilibrium MD simulations, for native ABL (WT, black line) and the 7 mutated variants (colored lines). The alignment was performed using the rigid C_{α} 's. The first frame of each equilibrium run served as reference for the RMSD. Both figures share the same legend. Residues are numbered according to the UniprotKB accession number P00519 (tyrosine-protein kinase ABL1).

Q252H equilibrium run for the definition of its average bound COM position $\mathbf{r}_{\text{COM}}^{\text{bound}}$.

Pulling simulations to generate initial path

To create an initial path to start the path sampling, pulling simulations (steered MD) were performed with GROMACS using the PLUMED (72) extension (version 2.7.2). Care was taken to ensure that the pulling simulations did not introduce large artifacts in the dissociation pathways, which involved manually checking the trajectories and several reruns with optimized parameters. Artifacts were encountered in two ways. First, it was noticed that pulling without restraints on the protein resulted in the C-lobe and N-lobe separating (the hinge region completely opening up). Second, it was noticed that the pulling force and velocity should be chosen carefully. If these values are too high, the system does not have time to relax along the orthogonal degrees of freedom, which can greatly impact the equilibration time of REPPTIS.

Pulling trajectories were obtained by restraining the C_{α} 's of the rigid residues ($\kappa = 5000 \text{ kJ mol}^{-1} \text{ nm}^{-2}$) and by pulling along the order parameter λ with a moving restraint ($\kappa = 250 \text{ kJ mol}^{-1} \text{ nm}^{-2}$) aimed to displace imatinib 38 \AA from the bound position in 50 ns (i.e. a pulling velocity of 0.76 \AA ns^{-1}).

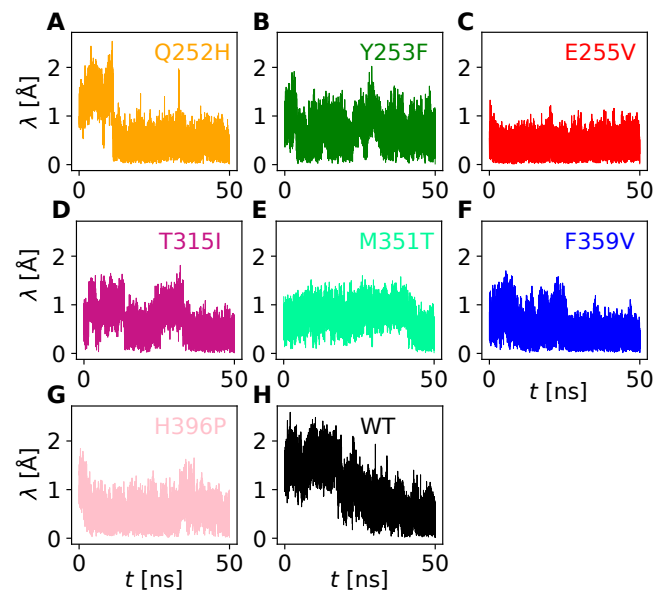


Figure 3: Order parameter λ (Eq. 2) for equilibrium MD trajectories of the ABL variants.

As the pulling was done slowly, and λ is defined as the distance to the average bound state, it is expected that the pulling force was non-directional. Six of the variants escaped via a pathway under the αC -helix, while the Q252H and F359V variants had imatinib escape via a pathway under the P-loop (Text S3, Fig. S3). The evolution of the order parameter λ during pulling is shown in Figs. 4A-B. The quick jumps in the dissociation are seen to be conserved in the variants (Fig. 4B). If the pulling force is too high, this plot would contain straight lines, where dissociation is more likely to sample unlikely pathways. Imatinib is strongly bound in the binding pocket of ABL, as suggested by a sudden transition (jump in λ) around the 5 ns to 10 ns mark, depending on the variant. Most of the variants do not simply display a single transition, and e.g. a double transition for WT ABL is clearly visible. This suggests the presence of metastable states, some of which have imatinib still strongly bound to ABL. Once imatinib transitions out of the deep binding pocket and its metastable states, the pulling profile is rather linear. This suggests that, at least for these pathways, the ligand was no longer strongly bound to the protein.

Trajectory-based order parameter calculation

Calculation of λ for a frame of the MD trajectory that is currently being generated involves (1) loading of the MD frame, (2) undoing PBC effects (making the protein and ligand whole), (3) aligning the frame onto a reference, and (4) calculating a distance. For such compute-heavy order parameters, the MD engine may be significantly faster than the λ -calculation. We have constructed a trajectory-based λ -calculation scheme where the order parameter is calculated for subtrajectories

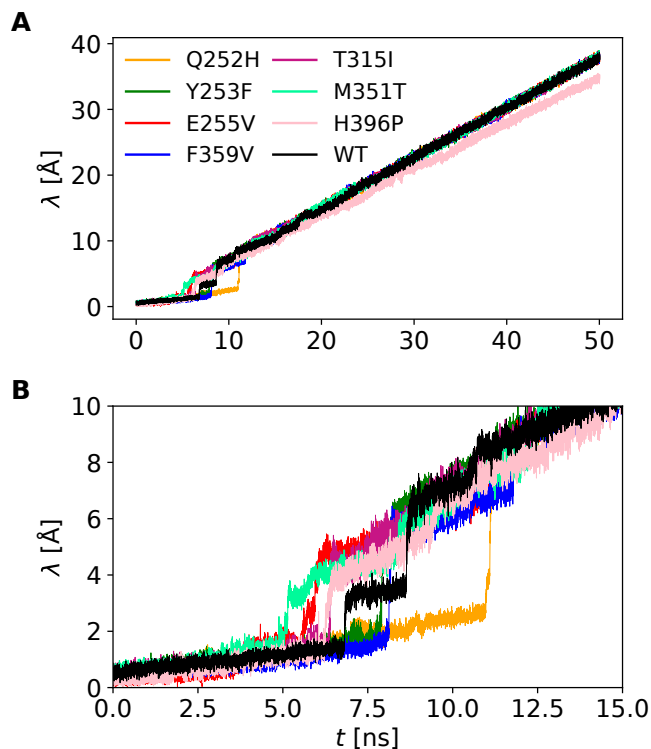


Figure 4: Pulling simulations of 50 ns, for each variant. **A**: Order parameter λ . **B**: Zoom-in on the first 15 ns of dissociation, showing ‘jumping’ behavior typical of activated processes. Native ABL (black line) shows a double transition, indicating the presence of a strongly bound metastable state.

of MD frames. As most of the four subroutines have implementations that are heavily optimized for trajectories of frames rather than frame-by-frame calculations, the resulting order parameter calculation was approximately 50-fold faster for the ABL-imatinib system. A detailed description of this calculation scheme is given in Text S2.

Asynchronous REPPTIS

Initially, RETIS was used to study the whole ABL-imatinib unbinding pathway using the PyRETIS 2 code (73). However, imatinib got trapped in a metastable state in many of the trajectories, preventing imatinib to unbind in a reasonable simulation time. In practice, a maximum path length is set in the PyRETIS algorithm. Paths exceeding this length are forcefully rejected to restrict disk space usage, and their occurrence should be minimal. In the RETIS simulations, nearly all shooting moves or wire-fencing moves resulted in trajectories that did not commit to λ_A or λ_B within the maximum allowed path length, even for values as high as 50 ns. This confirmed the presence of long-lived metastable states along the dissociation pathways, as predicted by the pulling and equilibrium simulations. The extremely low acceptance rate made RETIS infeasible and no results could be produced for the full un-

binding kinetics. The partial paths in the REPPTIS approach offer an answer to those long trajectories seen in RETIS, as the paths are cut short before they have fully committed to the bound or unbound state.

Further large speed-up of the REPPTIS simulations was achieved by implementing REPPTIS in a custom version of the infRETIS software (74). The ∞ RETIS (34, 57) algorithm allows multiple *workers* to run MD moves (or other MD intensive moves) in parallel, performing the MC moves of the path sampling algorithm asynchronously. This implementation was intended solely for the ability to use more hardware resources, as the infinite swapping formalism is not applicable to REPPTIS ensembles. The software was (successfully) tested for usage with the internal PyRETIS engine and the external GROMACS engine. Our custom version allowed to run REPPTIS asynchronously on multiple GPU and CPU simultaneously, leading to a linear speed-up with computational resources.

RESULTS

REPPTIS simulations

REPPTIS was used to study the whole imatinib unbinding pathway with the PyRETIS 3 code (75), for which the key input parameters are shown in Fig. S7. Order parameters were calculated every 40 fs ($n_{\text{subcycles}} = 20$), and the maximum path length was set to 4 ns. Occurrences of reaching the maximum path length were rare, as they only happened [0, 0, 1, 3, 3, 25, 0, 7] times for the [WT, Q252H, Y253F, E255V, F359V, T315I, M351T, H396P] variants. For all variants, 46 interfaces were used, where the first interfaces are closely spaced (deep binding pocket) and then gradually spaced further apart (Fig. S7). The steered MD simulations were used to initialize the REPPTIS path ensembles. Swap moves were attempted for 25% of the MC moves, and the remaining 75% were shooting moves.

The results of these simulations are shown in Table 2, where the initial path was excluded from the analysis. None of the simulations converged to a reliable rate estimate, where most did not contain sufficient data to calculate the global crossing probability $P_A(\lambda_B|\lambda_A)$ and the rate constant k_{AB} . Reliable nonzero estimates require at least one trajectory in each ensemble i beyond the initialization phase. If any ensemble fails to meet this criterion, estimating the global crossing probability—and consequently the rate—becomes unfeasible, which was the case here. Moreover, while a rate constant and error estimate was obtained for the E255V and T315I variants, their values are not reliable due to failed sampling in a large portion of the path ensembles (‘problematic ensembles’ column of Table 2), which is discussed in more detail in the next section. These ensembles likely failed to sample representative paths, resulting in extremely small (or zero-valued) local crossing probabilities. Nevertheless, to get an

| variant | N_{MC} | N_{ACC} | problematic ensembles | $P_A(\lambda_B \lambda_A)$ [10^{-27}] | f_A [ps $^{-1}$] | k_{AB} [s $^{-1}$] |
|---------|-------------|-------------------------------|-------------------------------------|--|------------------------------------|------------------------------------|
| WT | 53967 | 15003 | [0 – 15], 19, 25, 29, 36, [40 – 41] | <i>a</i> | $4.2 \cdot 10^{-2}$ $\pm 19\%$ | <i>a</i> |
| Q252H | 7156 | 2499 | [0 – 45] | <i>a</i> | <i>a</i> | <i>a</i> |
| Y53F | 45642 | 19402 | [0 – 16], 38 | <i>a</i> | $2.4 \cdot 10^{-1}$ $\pm 9.3\%$ | <i>a</i> |
| E255V | 72283 | 32597 | [0 – 10], 30, 31 | 1.3 $\pm 70\%$ | $1.6 \cdot 10^{-2}$ $\pm 30\%$ | $2.1 \cdot 10^{-17}$ $\pm 76\%$ |
| T315I | 108733 | 46370 | [0 – 15], [34 – 36] | 32 $\pm 53\%$ | $9.6 \cdot 10^{-3}$ $\pm 21\%$ | $3.1 \cdot 10^{-16}$ $\pm 57\%$ |
| M351T | 44451 | 21481 | [0 – 6], 17, 20, 21, 27 | <i>a</i> | $9.8 \cdot 10^{-1}$ $\pm 24\%$ | <i>a</i> |
| F359V | 17157 | 6006 | [0 – 45] | <i>a</i> | $1.6 \cdot 10^{-3}$ $\pm 85\%$ | <i>a</i> |
| H396P | 62497 | 17694 | [0 – 4], 18, 19, 32, 33, [40 – 42] | <i>a</i> | $2.6 \cdot 10^{-3}$ $\pm 31\%$ | <i>a</i> |
| variant | method | k_{off} [s $^{-1}$] | | | | |
| WT (76) | experiment | $(2.2 \pm 4.6) \cdot 10^{-3}$ | | | | |
| WT (77) | experiment | $(8.3 \pm 0.8) \cdot 10^{-4}$ | | | | |
| WT (78) | experiment | $(2.5 \pm 0.6) \cdot 10^1$ | | | | |
| WT (79) | milestoning | $1.8 \cdot 10^1$ | | | | |
| WT (80) | InMetaD | $(6 \pm 3) \cdot 10^{-4}$ | | | | |

Table 2: Results of the ABL-imatinib REPPTIS simulations (top half of table) and rate estimates from literature (bottom half of table). None of the simulations have converged to a reliable rate constant. All simulations used 46 ensembles. N_{MC} and N_{ACC} denote the number of MC moves performed and the number of MC moves accepted, respectively. Problematic ensembles are discussed in the text. *a*: Indicates that insufficient data were collected to determine the value. The provided errors were calculated using the recursive block averaging approach (75) based on one standard deviation. However, for unconverged simulations, they primarily reflect variance in the data rather than providing reliable confidence intervals for the computed mean values.

idea of the crossing probability profiles $P_A(\lambda_i|\lambda_A)$, the zero-valued local crossing probabilities were artificially set to 0.01, where the complementary local crossing probabilities were then set to 0.99 to keep their sum at 1 (e.g. $p_i^{\pm} + p_i^{\mp} \equiv 1$). The resulting profiles are shown in Fig. 5.

Causes of REPPTIS sampling issues

First, a note on the rate error estimations is warranted. While the error estimates for the E225V and T315I rates, 76% and 57%, give the impression of well-converged simulations, this is not the case. These rate estimates are based on the recursive block error approach (75), and, like any other error estimators, become unreliable when the underlying data itself is poor. This is because the approach assumes convergence that may not be present, causing the estimated error to be much smaller than the actual variability. To conclude, the precision of the rate estimates is likely severely overestimated.

Table 2 includes a list of the problematic ensembles. For all the simulations, these include the ensembles close to the deep binding pocket (small λ values), and some ensembles further along the unbinding pathway. This was not due to a severe lack of accepted paths in these ensembles, as there is no large discrepancy between the number of accepted paths

$N_{ACC}(i)$ for the different ensembles (Fig. 6).

Two other factors are believed to contribute to the sampling challenges. First, the Monte Carlo moves designed to promote progress along the one-dimensional order parameter λ are ineffective at facilitating exploration in orthogonal degrees of freedom. As a result, some ensembles encounter significant energy barriers along λ^{\perp} (i.e., directions orthogonal to λ), which can be crucial or even dominant for the dissociation process. Alternatively, the system may bypass these orthogonal barriers during the actual transition through diffusion within the reactant well along orthogonal directions before advancing along λ . This then couples with the second main issue, where the initial path may not have been representative of a true unbiased pathway. The orthogonal barriers then hinder the path sampling procedure to explore the relevant regions of phase space. As an example, it may be possible that a rotation of a dihedral angle between imatinib rings is the rate limiting step close to the deep binding pocket. If this rotation is missed in the initial path, then it is unlikely to be introduced by the sampling procedure if this rotational energy barrier is large.

These issues have been shown (81) to be substantially less pronounced in transition interface sampling (TIS) compared to other methods relying on a one-dimensional order

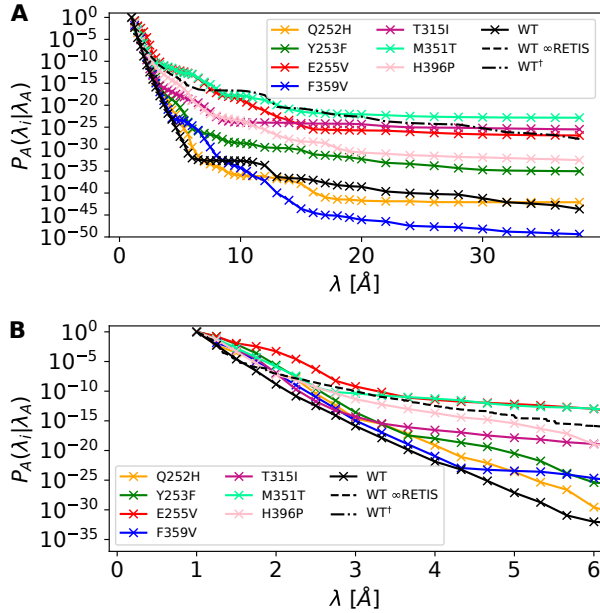


Figure 5: Crossing probability profile $P_A(\lambda_i|\lambda_A)$ for the ABL-imatinib systems (A) over the entire $\lambda \in [1, 38]$ Å range and (B) zoomed in on the $\lambda \in [1, 6]$ Å range. Profiles related to the REPPTIS simulations (lines with X-markers for each interface) have artificially assigned local crossing probabilities in case of zeros (see main text). The black dashed line denotes the ∞ RETIS simulation. The black dash-dotted line (WT[†]) is constructed by appending the $\lambda \in [6, 38]$ Å profile of WT REPPTIS to the $\lambda \in [1, 6]$ Å profile of WT ∞ RETIS.

parameter, such as forward flux sampling (FFS) (82), umbrella sampling (US), metadynamics with a single collective variable, or methods based on a dividing surface, like the Bennett-Chandler method (83). The incorporation of replica exchange in RETIS further mitigates these challenges. For instance, RETIS successfully captured distinct parallel transition channels in a permeation study (43), where orthogonal diffusion was enhanced using tailored Monte Carlo moves in the $[0^-]$ ensemble, specifically designed for such systems. These moves significantly improved sampling efficiency across all ensembles by leveraging the interconnectedness of replica exchange moves. However, the shorter trajectories in PPTIS are inherently more local and thus more prone to getting trapped than those in TIS and RETIS. Additionally, the replica exchange moves in REPPTIS are evidently insufficient to fully resolve this issue, highlighting the need for further enhancements to address orthogonal barriers.

The average path length $\langle \tau \rangle_i$ of each ensemble i , $\forall i \in \{1, \dots, 46\}$, is also shown in Fig. 6, for each of the variants. The path length is measured in ‘number of phasepoints’, where the starting and ending phase points of paths are excluded, and the average takes into account the weight of the path in the MC procedure. The path lengths are much lower near the

binding pocket, which is to be expected as the energy barrier is steepest in this region, and trajectories easily fall back into the reactant state. As the occurrence of paths that reach their right-most interface is rare in these ensembles, the REPPTIS swap move, which is a replica exchange MC move designed to improve phase space exploration, was rarely performed.

Let us now focus on WT ABL, whose crossing probability profile $P_A(\lambda_i|\lambda_A)$ showed the fastest drop of all the variants (Fig. 5). Path lengths for the WT ABL system in the $[1^+], \dots, [16^+]$ ensembles (ensemble indices 3 to 18 on Fig. 6N) vary around 20, with approximately 250 accepted paths per ensemble. This corresponds to $20 \times 40 \text{ fs} \times 250 = 200$ ps of combined trajectory lengths, for each of these ensembles. Only a fraction of this time can be seen as ‘equilibration time’, as the shooting points are (on average) not located near the beginning or end of paths. It is suspected that the initial path of WT ABL was not representative for the dominant reaction pathway, where the steered MD simulation pulled it along a barrier orthogonal to λ . This barrier was then not overcome by the fraction of the 200 ps of phase space exploration. Therefore, the local crossing probabilities p_i^\pm in these ensembles remain extremely low (or zero). For problematic ensembles further along the unbinding pathway ($[i^\pm]$, with $i \geq 20$), the path lengths are considerably longer.

Moreover, the efficiency of phase space and path space exploration is influenced not only by the path lengths but also by correlations between successive trajectories. These correlations arise because successive trajectories are likely confined to the same reaction channel, a consequence of the high orthogonal energy barriers. For these ensembles, such orthogonal barriers are expected to hinder efficient sampling of the corresponding $[i^\pm]$ path spaces. For the 6 mutants with initial paths dissociating under the α C-helix (Text S3, Fig. S3), this means that a converged simulation would likely only capture the rate associated with escape under the α C-helix, and not a ‘net’ rate taking into account possible dissociation pathways under/along the P-loop. This reasoning extends to the other mutated variants as well but is expected to be less pronounced in TIS and even less so in RETIS and ∞ RETIS, where enhanced sampling techniques mitigate these challenges.

∞ RETIS simulations

To further investigate the sampling issues close to the binding pocket, an ∞ RETIS simulation was run for the WT ABL system for the $\lambda \in [1, 6]$ Å range, focusing on the steep free energy increase associated to the first part of the imatinib unbinding pathway. The input parameters used for the ∞ RETIS simulation of WT ABL are shown in Fig. S8. Order parameters were calculated every 1 ps ($n_{\text{subcycles}} = 500$), and the maximum path length was set to 100 ns. Interfaces were placed from $\lambda_A = 1$ Å to $\lambda_B = 6$ Å with a separation of 0.1 Å, resulting in 51 interfaces and 51 ensembles $[0^-], [0^+], [1^+], \dots, [49^+]$. The interfaces can be put in closer proximity to each other,

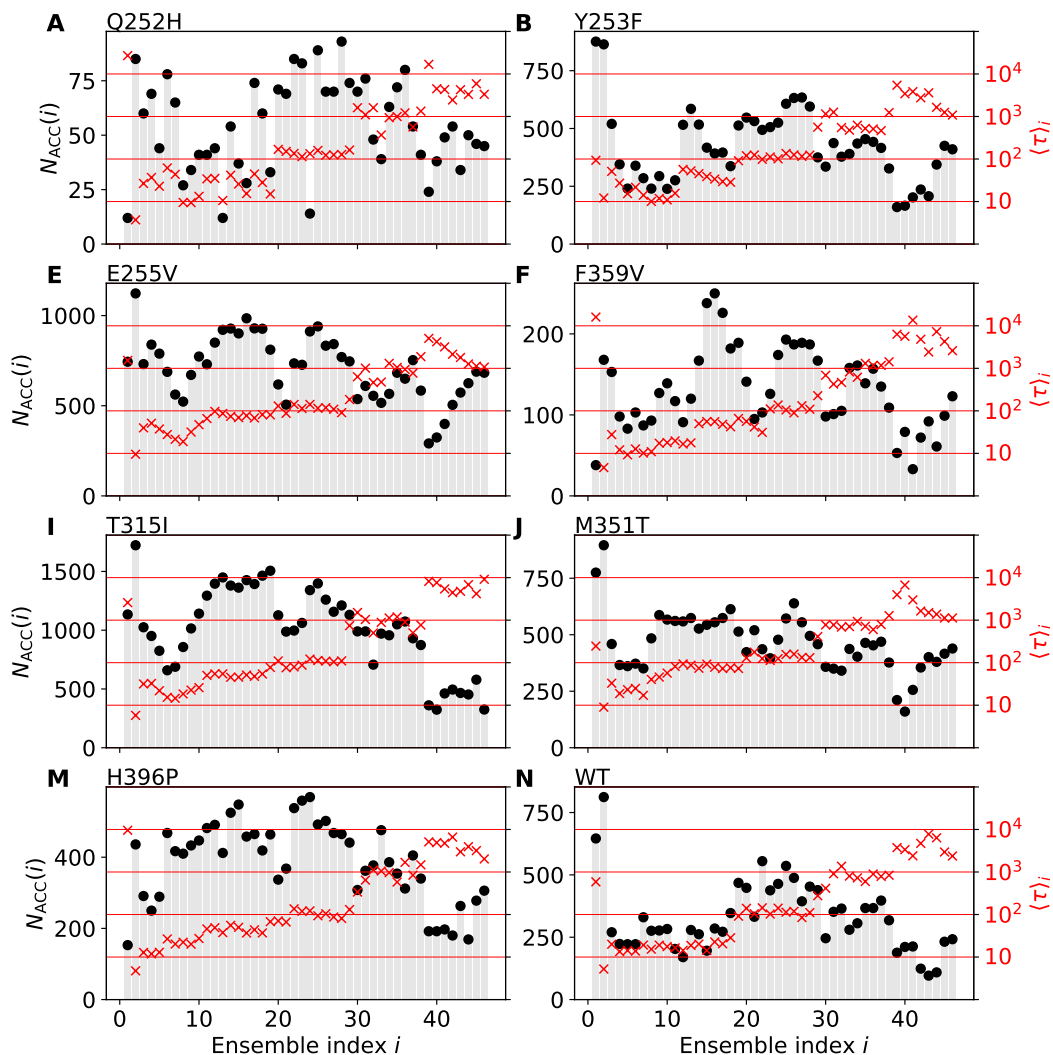


Figure 6: Analysis of REPPTIS simulations with 46 ensembles for each variant. Ensemble index 1 corresponds to $[0^-]$, index 2 to $[0^+]$, index 3 to $[1^+]$, etc. Left y-axis: number of unique accepted paths $N_{\text{ACC}}(i)$ in ensemble with index i is shown with gray bar and black dot; different scale for different variants. $N_{\text{ACC}}(i)$ denotes the number of accepted paths, i.e. the number of unique paths generated by a shooting move or replica exchange moves in REPPTIS. Right y-axis: average path length $\langle \tau \rangle_i$ is shown with red X-mark, which represents the average duration of the short unbiased trajectories in ensemble i . $\langle \tau \rangle_i$ is here measured in the number of phase points. Path phase points are separated by 40 fs, so a path length value of e.g. 100 represents 4 ps. The same logarithmic scale is used for all variants.

as the infinite swapping formalism of ∞ RETIS efficiently distributes (swaps) path information between the ensembles. Furthermore, the optimal number of workers (MD intensive moves that can run in parallel) is approximately half of the number of ensembles, where it is thus advantageous to place more interfaces than what is standard for a PyRETIS simulation using the RETIS algorithm.

The resulting crossing probability profile $P_A(\lambda|\lambda_A)$ is included in Fig. 5A-B (black dashed line) for comparison with the REPPTIS profiles, and also shown separately in Fig. 7A. The first 5000 of the 18 070 accepted paths were discarded in the analysis to reduce initialization effects. The weighted

histogram analysis (WHAM) method approach of RETIS produces a continuous crossing probability profile, rather than discrete points at the interface positions for REPPTIS. The drop in crossing probability is dramatically less steep than the WT REPPTIS profile with about 16 orders of magnitude. However, discontinuities in the $P_A(\lambda|\lambda_A)$ profile are visible (arrow indications on Fig. 7A), and are discussed next.

The discontinuity around $\lambda \approx 1.9 \text{ \AA}$ is due to the under-sampling of far-reaching trajectories in the first 9 positive ensembles $[0^+], \dots, [8^+]$. The average paths lengths of these ensembles (now measured in ps, as $n_{\text{subcycles}} \times \text{timestep} = 1$ ps) is too small to promote equilibration by phase space ex-

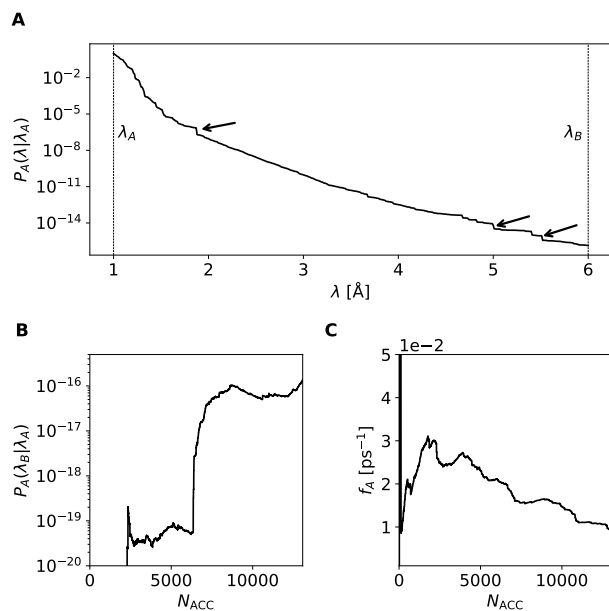


Figure 7: WT ABL ∞ RETIS results, where the first 5000 accepted paths were discarded to reduce initialization effects. **A:** The crossing probability profile $P_A(\lambda|\lambda_A)$ of Eq. 1. Arrows indicate visible discontinuities. **B:** The running estimate of the global crossing probability $P_A(\lambda_B|\lambda_A)$ shows a large jump, hinting at non-convergence of the simulation. **C:** The running estimate of the flux f_A of Eq. 1. N_{ACC} denotes the number of accepted paths i.e. the number of unique paths generated by a shooting move.

ploration (Fig. 8B). Most of the paths in these ensembles consist of only a single phase point. Algorithmically, this is equivalent to paths containing three phase points, where the first and last points are not a part of the path ensemble (they belong to state A or B) and therefore excluded from being viable shooting points. This means that, for these 1-phase point paths, the configuration remains identical as only the momenta are modified. It is clear that decorrelation between paths is extremely slow when there is only one phase point available to shoot from. Thus, despite the high acceptance rate of paths in these ensembles (Fig. 8A), exploration of the ensemble’s path space remains sluggish due to the strong correlation among shooting points.

The discontinuities in $P_A(\lambda|\lambda_A)$ for $\lambda \geq 4.5$ Å arise due to the limited number of accepted paths (≤ 100) in the corresponding ensembles (Fig. 8A), despite each ensemble having simulated approximately 500 ns or more of shooting time (Fig. 8C). This low acceptance could have been mitigated using the wire-fencing move with high-acceptance (39), a recent advanced shooting move designed to improve decorrelation and achieve near rejection-free sampling, particularly for ensembles close to the reactant state. Such a move would likely enhance the exploration of under-sampled path spaces

and improve the convergence of the corresponding ensembles. However, we will investigate in future studies whether this approach also resolves issues arising from occurrences when there is only one phase point to shoot from.

Based on the observed variation in path lengths, it is clear that metastable states are present in the WT ABL-imatinib system, even for order parameter values as low as $\lambda = 2$ Å. This suggests that the separation of timescales introduced by these states might fundamentally *not* be resolvable by a one-dimensional λ -based approach. Specifically, a return to state A from $\lambda \geq 2$ Å can occur within just a few RETIS timesteps of 1 ps—or even a single timestep—when no metastable state is encountered. Conversely, when the trajectory becomes trapped in a metastable state, returning to state A can take thousands of timesteps. This highlights the inherent limitations of relying on a single reaction coordinate to capture the complexities of the dynamics involved. The importance of the order parameter choice on simulation convergence is further discussed in the Discussion section, together with alternative order parameter definitions that may provide better performance for complex protein-drug systems like ABL-imatinib.

Although ∞ RETIS shows a significant improvement over REPPTIS, and even more so over PPTIS, in handling a single λ parameter for enforcing progress, and despite the potential for further efficiency gains with advanced shooting moves, the very large average path lengths observed for ensembles beyond 6 Å make this approach currently unfeasible. A (RE)PPTIS or milestone approach seems more practical under these conditions.

A strategy could be to combine both methods, in order to leverage the better sampling efficiency of ∞ RETIS at the start and the shorter path length of REPPTIS further along the reaction. As indicated by the black dash-dotted line in Fig. 5), we extended the ∞ RETIS crossing probability profile with the $\lambda \in [6, 38]$ Å range from the WT REPPTIS simulation. This gives a global crossing probability $P_A(\lambda_B|\lambda_A)$ of 2.08×10^{-28} . When combined with the WT ABL flux from ∞ RETIS ($9.51 \times 10^{-3} \text{ ps}^{-1}$), the resulting rate estimate for imatinib dissociation from WT ABL is $1.98 \times 10^{-18} \text{ s}^{-1}$. This estimate, despite being 16 orders of magnitude higher than the pure REPPTIS result, remains more than 10 orders of magnitude lower than experimental measurements.

It is noteworthy that the variation among experimental results, as summarized in Table 2, spans nearly five orders of magnitude, and also simulation-based approaches, based on milestone and infrequent metadynamics, differ by nearly five orders of magnitude. Although these variations are large, they are still significantly closer to each other than to the combined ∞ RETIS-REPPTIS estimate. The large underestimation of the crossing probability in our simulation is likely not only the result of force field discrepancies, but more importantly the result of sampling issues, as discussed below.

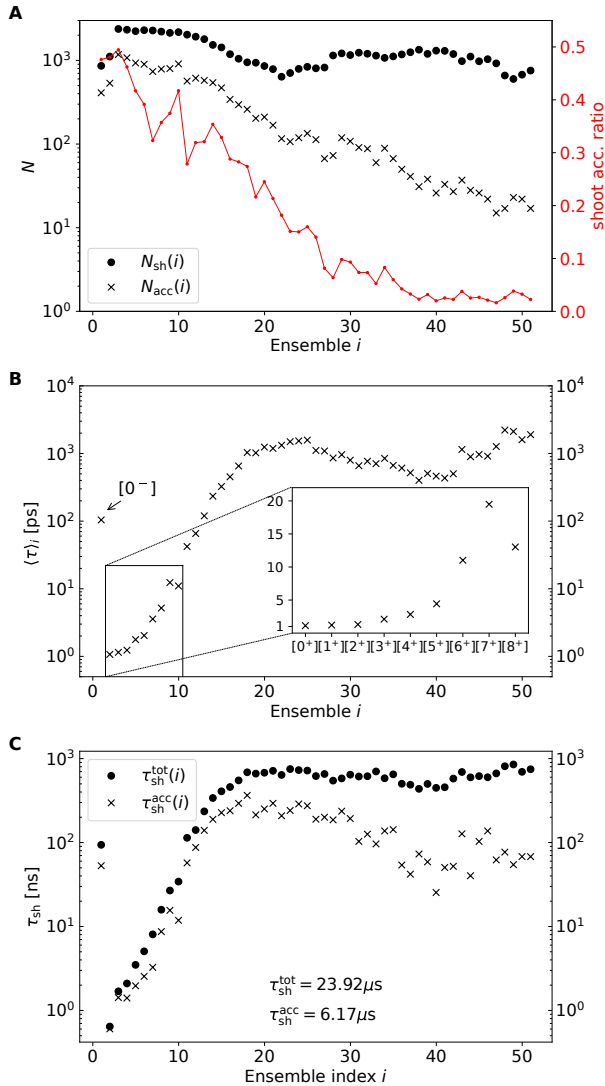


Figure 8: Sampling analysis of the ∞ RETIS WT ABL simulation. All *shooting* cycles are included in the analysis, i.e. paths generated by the zero swap move in $[0^-]$ and $[0^+]$ are excluded. Ensemble index 1 corresponds to $[0^-]$, ensemble index 2 to $[0^+]$, ensemble index 3 to $[1^+]$, etc. **A:** $N_{sh}(i)$ is the number of performed shooting moves in the ∞ RETIS simulation, both accepted and rejected (black dots). $N_{acc}(i)$ is the number of accepted shooting moves (black crosses). The acceptance ratio is shown in red. **B:** Average path length $\langle\tau\rangle_i$, representing the ensemble average duration of the short unbiased paths of ensemble i . **C:** The total amount of simulated (shooting) time $\tau_{sh}^{tot}(i)$ (dots) and the accepted portion $\tau_{sh}^{acc}(i)$ thereof (crosses). Path length is measured as the number of phase points of the path, which are saved every 1 ps. E.g. a path length of 100 corresponds to 100 ps.

DISCUSSION

Both RETIS and REPPTIS faced significant challenges in achieving well-converged kinetics for imatinib dissociation

from ABL. These challenges most likely stem from the complexity of the unbinding mechanism, where the Monte Carlo exploration of path space struggles to adequately sample along directions orthogonal to the reaction coordinate λ . This orthogonal sampling is crucial because spontaneous dynamical transitions may involve crossing orthogonal barriers, leading to alternative pathways with potentially lower barriers along λ . Although these routes might not initially appear as paths of least resistance, they can ultimately result in more favorable dissociation trajectories.

For REPPTIS, barriers orthogonal to λ prevent paths from equilibrating within the relevant regions of path space. If the initial path segments (paths truncated to the $[i^\pm]$ ensemble boundaries) are not representative of a true dissociating pathway, the short path lengths and the strict locality of the path ensemble definitions hinder the exploration of relevant path space, particularly for ensembles near the binding pocket. This issue is exacerbated by the low acceptance of replica exchange moves, which are crucial for facilitating transitions along orthogonal degrees of freedom. The steepness of the orthogonal energy barriers results in most trajectories returning to λ_{i-1} after reaching λ_i from λ_{i-1} , with few successfully advancing to λ_{i+1} . Since paths returning to λ_{i-1} cannot be swapped with a path in the $[(i+1)^\pm]$ ensemble, the replica exchange acceptance rate is low.

While ∞ RETIS improved sampling in the $\lambda \in [2, 6]$ Å region, the separation of timescales necessitates a significantly smaller timestep (as defined by $n_{subcycles}$, the number of MD steps that comprise a full TIS timestep) for effective sampling in the $\lambda \in [1, 2]$ Å region. This higher saving frequency would result in substantially larger disk space usage and extended simulation times due to increased data-writing overhead. An even larger problem is that setting $\lambda_B = 6$ Å does not ensure full dissociation. Increasing λ_B would introduce exceptionally long paths as imatinib is frequently (transiently) trapped in metastable states between the binding pocket and solvent. Methods such as (RE)PPTIS and milestoning are better suited for handling dynamics that are both rare and slow. However, the validity of the Markovian assumption implied by (RE)PPTIS depends on the choice of order parameter.

The selection of an appropriate order parameter λ is critical for all enhanced sampling methods, as it can influence both computational efficiency and the results upon convergence. For (RE)PPTIS and Milestoning, an unfavorable choice of λ can compromise Markovianity, where results diverge from those expected from (extremely long) MD simulations. While other methods will, in principle, yield exact results regardless of λ , a poor choice of λ can result in an exponential increase in computational cost. TIS and RETIS, in this respect, theoretically offer an advantage over splitting-based methods such as forward flux sampling, weighted ensemble method (84), and adaptive multilevel splitting (85) and Bennett-Chandler-type approaches, as their efficiency is less sensitive to the order parameter. This advantage has been demonstrated for simple 1D and 2D model systems (26, 81). However, in complex,

high-dimensional systems, the choice of λ is likely to remain crucial, even for these methods.

When slow (diffusive) or rare (energetic) barriers important to the reaction mechanism are not captured by λ , then convergence can become drastically problematic, as was the case for the simple one-dimensional distance λ parameter used in this ABL-imatinib study. Alternative one-dimensional λ parameters may be better suited for complex protein-drug dissociation studies. A contact map parameter based on hydrogen bond donor/acceptor distances between the protein and drug may capture important steps in the dissociation mechanism that are not accompanied by a simple displacement from the native binding pose. Such a parameter was successfully used in studying the association and dissociation of protein-DNA complexes (41, 86) and may also be better suited here. Another alternative is to employ path collective variables (PCVs) that tackle a specific dissociative pathway for each of the ABL mutants. Such a pathway can be constructed via the string method (87, 88), or via machine-learning methodologies that, for example, employ autoencoders to construct a PCV using a low-dimensional representation of the system (89–91). The ABL-imatinib simulations in this work showed that the addition of replica exchange to the PPTIS framework was unable to alleviate the crucial dependency of the convergence speed on λ , and going forward it will be rewarding to allocate compute time on suitable λ design prior to running the costly RE(P)TIS drug dissociation simulations.

Long MD simulations on the special purpose Anton 2 supercomputer have revealed that there are a multitude of long-lived metastable states, even close to and within the deep binding pocket (66, 92). While the presence of metastable states is not problematic for REPPTIS, kinetic analysis of the ABL-imatinib system in the recent works of Refs. (79, 80) suggested that the dissociation process requires a multidimensional description in collective variable spaces and that a one-dimensional order parameter is fundamentally not sufficient. A multidimensional milestone method was used by Elber et al. (79), where Voronoi tessellation revealed a milestone network with average connectivity of 2.93, whereas a value of 2 is expected for a one-dimensional description. Infrequent metadynamics simulations by Shekhar et al. (80) used a 5-dimensional reaction coordinate model to extract the rate constant of the ABL-imatinib system. The results of these studies were also included in Table 2, and are in much closer agreement with the few experimental values available. The study of Shekhar et al. (80) also found that, in wild type ABL, imatinib predominantly dissociates through a route near the kinase hinge region, which is a pathway that becomes accessible following the disruption of a hydrogen bond between Y253 (from the P-loop) and N322 (from the hinge). In our study, the initial steered MD pathway generated for wild type ABL escaped under the α C-helix (Fig. S3), where the aforementioned hydrogen bond is not disrupted. As this hydrogen bond does not directly impact the order parameter (i.e. it is orthogonal to λ), its disruption is hard to sample

in REPPTIS. Similarly, changes in characteristic motifs of (mutated) ABL structures are expected not to be captured by λ , resulting in impeded path sampling.

To summarize, while the Monte Carlo approach to path generation is a key strength of REPPTIS as initial paths naturally evolve to representative paths via importance sampling, this ‘path equilibration’ process is impeded when orthogonal barriers are too high, and more so when replica exchange is frustrated due to a steep slope along λ . While improved initial path generation might have enhanced the convergence of the ABL-imatinib REPPTIS simulations, it may also indicate that REPPTIS needs to be generalized to a multidimensional order parameter to address this and similarly complex biological systems.

FUTURE PERSPECTIVES AND CONCLUSION

Future work will focus on combining REPPTIS with multiple-state TIS (93), where metastable state definitions could be derived from a Voronoi tessellation approach similar to that used in directional milestone or from recent machine learning algorithms like Vampnets (94). In particular, partially retaining the memory effect inherent to REPPTIS may be advantageous by relaxing the requirements for defining anchoring points in the tessellation or the boundaries of metastable states in collective variable space. This is because, in the PPTIS formalism, transitions between states do not need to be strictly Markovian.

In addition, it is interesting to increase the memory so that the terminating boundaries in the ensemble centered around λ_i are not necessarily limited to the neighboring interfaces λ_{i+1} and λ_{i-1} , but can extend to interfaces that are further away. This concept has already been tested in simple toy systems (95) but could also be combined with a multidimensional order parameter network. Such an approach could eventually provide a seamless connection between ∞ RETIS and REPPTIS, beyond the *ad hoc* method used here. This would allow path ensembles to adapt and treat different characteristics of the free energy landscape in a way that aligns more closely with either ∞ RETIS or REPPTIS, depending on which method is best suited for the underlying free energy landscape.

We also plan to enhance the shooting move, where the high acceptance rates and rapid decorrelation of wire-fencing is preferable for future studies. However, our results suggest an alternative approach for high-dimensional systems. High frame-saving rates slow computation and increase disk space demands, while low rates limit the number of shooting points. Ideally, the frame-saving rate should be flexible. Wire-fencing could provide an elegant solution by incorporating a high frame-saving rate for the sub-trajectories, which are not sampled but serve as intermediates between the actual paths in the Monte Carlo approach, while maintaining a lower frame-saving rate for the actual paths.

The orthogonal sampling could be further enhanced by run-

ning metadynamics simulations in parallel and incorporating replica exchange moves between metadynamics configurations and randomly selected shooting points from trajectories (96). This approach has the advantage that the λ parameter can remain low-dimensional, and in some cases one-dimensional, since the multidimensional diffusion and orthogonal barrier crossings primarily occur during the metadynamics simulations. The effects of these crossings are then transferred to the path ensembles via the swapping moves.

In summary, while the challenges posed by orthogonal barriers and high-dimensional systems remain significant, the methodologies discussed here offer promising pathways to enhance sampling and facilitate the exploration of complex molecular processes. Future advancements, such as the integration of multidimensional order parameters and improved sampling techniques like wire-fencing and parallel metadynamics, are poised to refine these approaches further. By leveraging these strategies, we can advance our ability to capture rare events and transition pathways, ultimately contributing to a deeper understanding of molecular dynamics and complex biological systems.

Supplemental Information

Additional details are provided in the Supplemental Information, including Figures S1-S6, Table S1, and Texts S1-S3.

Code availability

Analysis was performed using [PyRETIS](#) and [infertools](#). The custom version of ∞ REPPTIS is available on request. The configurations and topology files of the ABL-imatinib systems are available on Zenodo (97).

Author contributions

WV developed the simulation protocol, ran simulations, and performed the analysis. DTZ and ER assisted in software development and running of simulations. TvE assisted in developing the simulation protocol. AG was responsible for the conceptualization and supervision. WV, TvE, and AG wrote the paper. All authors reviewed the paper.

Declaration of interests

The authors declare no competing interests.

Acknowledgments

The computational resources (Stevin Supercomputer Infrastructure) and services used in this work were provided by the VSC (Flemish Supercomputer Center), funded by Ghent University, FWO and the Flemish Government – department EWI. AG acknowledges funding of the FWO (project G002520N and project G094023N) and the European Union (ERC Consolidator grant, 101086145 PASTIME).

REFERENCES

1. Lipinski, C. A., F. Lombardo, B. W. Dominy, and P. J. Feeney, 2012. Experimental and computational approaches to estimate solubility and permeability in drug discovery and development settings. *Adv. Drug Deliv. Rev.* 64:4–17.
2. Jorgensen, W. L., 2004. The many roles of computation in drug discovery. *Science* 303:1813–1818.
3. Claveria-Gimeno, R., S. Vega, O. Abian, and A. Velazquez-Campoy, 2017. A look at ligand binding thermodynamics in drug discovery. *Expert Opin. Drug Discov.* 12:363–377.
4. Mobley, D. L., and M. K. Gilson, 2017. Predicting binding free energies: frontiers and benchmarks. *Annu. Rev. Biophys.* 46:531–558.
5. Copeland, R. A., D. L. Pompliano, and T. D. Meek, 2006. Drug–target residence time and its implications for lead optimization. *Nat. Rev. Drug Discov.* 5:730–739.
6. Tummino, P. J., and R. A. Copeland, 2008. Residence time of receptor–ligand complexes and its effect on biological function. *Biochem.* 47:5481–5492.
7. Copeland, R. A., 2010. The dynamics of drug–target interactions: drug–target residence time and its impact on efficacy and safety. *Expert Opin. Drug Discov.* 5:305–310.
8. Lu, H., and P. J. Tonge, 2010. Drug–target residence time: critical information for lead optimization. *Curr. Opin. Chem. Biol.* 14:467–474.
9. Copeland, R. A., 2016. The drug–target residence time model: a 10-year retrospective. *Nat. Rev. Drug Discov.* 15:87–95.
10. Wang, L., H. L. McLeod, and R. M. Weinshilboum, 2011. Genomics and drug response. *New England Journal of Medicine* 364:1144–1153.
11. Relling, M. V., and W. E. Evans, 2015. Pharmacogenomics in the clinic. *Nature* 526:343–350.
12. Sneha, P., and C. George Priya Doss, 2016. Chapter Seven - Molecular Dynamics: New Frontier in Personalized Medicine. In R. Donev, editor, *Personalized Medicine*, Academic Press, volume 102 of *Advances in Protein Chemistry and Structural Biology*, 181–224.
13. Georgoulia, P. S., G. Todde, S. Bjelic, and R. Friedman, 2019. The catalytic activity of Abl1 single and compound mutations: Implications for the mechanism of drug resistance mutations in chronic myeloid leukaemia. *Biochimica et Biophysica Acta (BBA)-General Subjects* 1863:732–741.

14. O'hare, T., M. S. Zabriskie, A. M. Eiring, and M. W. Deininger, 2012. Pushing the limits of targeted therapy in chronic myeloid leukaemia. *Nat. Rev. Cancer* 12:513–526.
15. Stegmeier, F., M. Warmuth, W. Sellers, and M. Dorsch, 2010. Targeted cancer therapies in the twenty-first century: lessons from imatinib. *Clin. Pharmacol. Ther.* 87:543–552.
16. Reddy, E. P., and A. K. Aggarwal, 2012. The ins and outs of bcr-abl inhibition. *Genes & cancer* 3:447–454.
17. Shoichet, B. K., 2004. Virtual screening of chemical libraries. *Nature* 432:862–865.
18. Okimoto, N., N. Futatsugi, H. Fuji, A. Suenaga, G. Morimoto, R. Yanai, Y. Ohno, T. Narumi, and M. Taiji, 2009. High-performance drug discovery: computational screening by combining docking and molecular dynamics simulations. *PLoS Comput. Biol.* 5:e1000528.
19. Jorgensen, W. L., 2009. Efficient drug lead discovery and optimization. *Accounts of chemical research* 42:724–733.
20. Lin, X., X. Li, and X. Lin, 2020. A review on applications of computational methods in drug screening and design. *Molecules* 25:1375.
21. Dellago, C., P. G. Bolhuis, F. S. Csajka, and D. Chandler, 1998. Transition path sampling and the calculation of rate constants. *J. Chem. Phys.* 108:1964–1977.
22. Bolhuis, P. G., D. Chandler, C. Dellago, and P. L. Geissler, 2002. Transition path sampling: Throwing ropes over rough mountain passes, in the dark. *Annu. Rev. Phys. Chem.* 53:291–318.
23. Bolhuis, P. G., and D. W. Swenson, 2021. Transition path sampling as Markov chain Monte Carlo of trajectories: Recent algorithms, software, applications, and future outlook. *Adv. Theory Simul.* 4:2000237.
24. Bolhuis, P. G., and D. W. H. Swenson, 2021. Transition Path Sampling as Markov Chain Monte Carlo of Trajectories: Recent Algorithms, Software, Applications, and Future Outlook. *Adv. Theory Simul.* 4:2000237.
25. Van Erp, T. S., D. Moroni, and P. G. Bolhuis, 2003. A novel path sampling method for the calculation of rate constants. *J. Chem. Phys.* 118:7762–7774.
26. Van Erp, T. S., 2012. Dynamical rare event simulation techniques for equilibrium and nonequilibrium systems. *Adv. Chem. Phys.* 151:27.
27. Faradjian, A. K., and R. Elber, 2004. Computing time scales from reaction coordinates by milestoning. *J. Chem. Phys.* 120:10880–10889.
28. Ojha, A. A., L. W. Votapka, and R. E. Amaro, 2024. Advances and Challenges in Milestoning Simulations for Drug–Target Kinetics. *Journal of Chemical Theory and Computation* 20:9759–9769. PMID: 39508322.
29. Moroni, D., P. G. Bolhuis, and T. S. van Erp, 2004. Rate constants for diffusive processes by partial path sampling. *J. Chem. Phys.* 120:4055–4065.
30. van Erp, T. S., 2007. Reaction rate calculation by parallel path swapping. *Phys. Rev. Lett.* 98:268301.
31. Bolhuis, P. G., 2008. Rare events via multiple reaction channels sampled by path replica exchange. *J. Chem. Phys.* 129.
32. Cabriolu, R., K. M. Skjelbred Refsnes, P. G. Bolhuis, and T. S. van Erp, 2017. Foundations and latest advances in replica exchange transition interface sampling. *J. Chem. Phys.* 147.
33. Vervust, W., D. T. Zhang, T. S. Van Erp, and A. Ghysels, 2023. Path sampling with memory reduction and replica exchange to reach long permeation timescales. *Biophys. J.* 122:2960–2972.
34. Zhang, D. T., L. Baldauf, S. Roet, A. Lervik, and T. S. van Erp, 2024. Highly parallelizable path sampling with minimal rejections using asynchronous replica exchange and infinite swaps. *Proc. Natl. Acad. Sci. U.S.A.* 121:e2318731121.
35. Moqadam, M., E. Riccardi, T. T. Trinh, A. Lervik, and T. S. van Erp, 2017. Rare event simulations reveal subtle key steps in aqueous silicate condensation. *Phys. Chem. Chem. Phys.* 19:13361–13371.
36. Moqadam, M., A. Lervik, E. Riccardi, V. Venkatraman, B. K. Alsberg, and T. S. van Erp, 2018. Local initiation conditions for water autoionization. *Proc. Nat. Acad. Sci. U.S.A.* 115:E4569–E4576.
37. Daub, C. D., E. Riccardi, V. Hänninen, and L. Halonen, 2020. Path sampling for atmospheric reactions: formic acid catalysed conversion of SO₃+ H₂O to H₂SO₄. *PeerJ Phys. Chem.* 2:e7.
38. Aarøen, O., E. Riccardi, T. S. van Erp, and M. Sletmoen, 2022. Thin film breakage in oil-in-water emulsions, a multidisciplinary study. *Colloids Surf. A Physicochem. Eng. Asp.* 632:127808.
39. Zhang, D. T., E. Riccardi, and T. S. van Erp, 2023. Enhanced path sampling using subtrajectory Monte Carlo moves. *J. Chem. Phys.* 158.
40. Lervik, A., I.-H. Svenum, Z. Wang, R. Cabriolu, E. Riccardi, S. Andersson, and T. S. van Erp, 2022. The role

- of pressure and defects in the wurtzite to rock salt transition in cadmium selenide. *Phys. Chem. Chem. Phys.* 24:8378–8386.
41. Riccardi, E., E. C. van Mastbergen, W. W. Navarre, and J. Vreede, 2019. Predicting the mechanism and rate of H-NS binding to AT-rich DNA. *PLoS Comput. Biol.* 15:e1006845.
 42. Riccardi, E., A. Krämer, T. S. van Erp, and A. Ghysels, 2020. Permeation rates of oxygen through a lipid bilayer using replica exchange transition interface sampling. *J. Phys. Chem. B* 125:193–201.
 43. Ghysels, A., S. Roet, S. Davoudi, and T. S. van Erp, 2021. Exact non-Markovian permeability from rare event simulations. *Phys. Rev. Res.* 3:033068.
 44. Panjarian, S., R. E. Iacob, S. Chen, J. R. Engen, and T. E. Smithgall, 2013. Structure and dynamic regulation of Abl kinases. *J. Biol. Chem.* 288:5443–5450.
 45. Simpson, G. L., S. M. Bertrand, J. A. Borthwick, N. Campobasso, J. Chabanet, S. Chen, J. Coggins, J. Cottom, S. B. Christensen, H. C. Dawson, et al., 2019. Identification and optimization of novel small c-Abl kinase activators using fragment and HTS methodologies. *J. Med. Chem.* 62:2154–2171.
 46. Xie, T., T. Saleh, P. Rossi, and C. G. Kalodimos, 2020. Conformational states dynamically populated by a kinase determine its function. *Science* 370:eabc2754.
 47. DeLano, W. L., et al., 2002. Pymol: An open-source molecular graphics tool. *CCP4 Newsl. Protein Crystallogr* 40:82–92.
 48. Shah, N. P., J. M. Nicoll, B. Nagar, M. E. Gorre, R. L. Paquette, J. Kuriyan, and C. L. Sawyers, 2002. Multiple BCR-ABL kinase domain mutations confer polyclonal resistance to the tyrosine kinase inhibitor imatinib (STI571) in chronic phase and blast crisis chronic myeloid leukemia. *Cancer cell* 2:117–125.
 49. Shah, N. P., B. J. Skaggs, S. Branford, T. P. Hughes, J. M. Nicoll, R. L. Paquette, C. L. Sawyers, et al., 2007. Sequential ABL kinase inhibitor therapy selects for compound drug-resistant BCR-ABL mutations with altered oncogenic potency. *The Journal of clinical investigation* 117:2562–2569.
 50. van Erp, T. S., 2023. How far can we stretch the timescale with RETIS? *EPL* 143:30001.
 51. Grünwald, M., C. Dellago, and P. L. Geissler, 2008. Precision shooting: Sampling long transition pathways. *J. Chem. Phys.* 129.
 52. Gingrich, T. R., and P. L. Geissler, 2015. Preserving correlations between trajectories for efficient path sampling. *J. Chem. Phys.* 142.
 53. Jung, H., K.-i. Okazaki, and G. Hummer, 2017. Transition path sampling of rare events by shooting from the top. *J. Chem. Phys.* 147.
 54. Menzl, G., A. Singraber, and C. Dellago, 2016. S-shooting: a Bennett–Chandler-like method for the computation of rate constants from committor trajectories. *Faraday Discussions* 195:345–364.
 55. Borrero, E. E., and C. Dellago, 2016. Avoiding traps in trajectory space: Metadynamics enhanced transition path sampling. *Eur. Phys. J. Spec. Top.* 225:1609–1620.
 56. Riccardi, E., O. Dahlen, and T. S. van Erp, 2017. Fast Decorrelating Monte Carlo Moves for Efficient Path Sampling. *J. Phys. Chem. Lett.* 8:4456–4460.
 57. Roet, S., D. T. Zhang, and T. S. van Erp, 2022. Exchanging replicas with unequal cost, infinitely and permanently. *J. Phys. Chem. A* 126:8878–8886.
 58. Jo, S., T. Kim, V. G. Iyer, and W. Im, 2008. CHARMM-GUI: a web-based graphical user interface for CHARMM. *J. Comput. Chem.* 29:1859–1865.
 59. Chan, W. W., S. C. Wise, M. D. Kaufman, Y. M. Ahn, C. L. Ensinger, T. Haack, M. M. Hood, J. Jones, J. W. Lord, W. P. Lu, et al., 2011. Conformational control inhibition of the BCR-ABL1 tyrosine kinase, including the gatekeeper T315I mutant, by the switch-control inhibitor DCC-2036. *Cancer cell* 19:556–568.
 60. Abraham, M. J., T. Murtola, R. Schulz, S. Páll, J. C. Smith, B. Hess, and E. Lindahl, 2015. GROMACS: High performance molecular simulations through multi-level parallelism from laptops to supercomputers. *SoftwareX* 1:19–25.
 61. Huang, J., S. Rauscher, G. Nawrocki, T. Ran, M. Feig, B. L. De Groot, H. Grubmüller, and A. D. MacKerell Jr, 2017. CHARMM36m: an improved force field for folded and intrinsically disordered proteins. *Nat. Methods* 14:71–73.
 62. Jorgensen, W. L., J. Chandrasekhar, J. D. Madura, R. W. Impey, and M. L. Klein, 1983. Comparison of simple potential functions for simulating liquid water. *J. Chem. Phys.* 79:926–935.
 63. Lin, Y.-L., Y. Meng, L. Huang, and B. Roux, 2014. Computational study of Gleevec and G6G reveals molecular determinants of kinase inhibitor selectivity. *J. Am. Chem. Soc.* 136:14753–14762.

64. Huang, L., and B. Roux, 2013. Automated force field parameterization for nonpolarizable and polarizable atomic models based on ab initio target data. *J. Chem. Theory Comput.* 9:3543–3556.
65. Boulanger, E., L. Huang, C. Rupakheti, A. D. MacKerell Jr, and B. Roux, 2018. Optimized Lennard-Jones parameters for druglike small molecules. *J. Chem. Theory Comput.* 14:3121–3131.
66. Paul, F., T. Thomas, and B. Roux, 2020. Diversity of long-lived intermediates along the binding pathway of imatinib to Abl kinase revealed by MD simulations. *J. Chem. Theory Comput.* 16:7852–7865.
67. Aleksandrov, A., and T. Simonson, 2010. A molecular mechanics model for imatinib and imatinib: kinase binding. *J. Comput. Chem.* 31:1550–1560.
68. Bussi, G., D. Donadio, and M. Parrinello, 2007. Canonical sampling through velocity rescaling. *J. Chem. Phys.* 126.
69. Parrinello, M., and A. Rahman, 1981. Polymorphic transitions in single crystals: A new molecular dynamics method. *J. Appl. Phys.* 52:7182–7190.
70. Hess, B., H. Bekker, H. J. Berendsen, and J. G. Fraaije, 1997. LINCS: A linear constraint solver for molecular simulations. *J. Comput. Chem.* 18:1463–1472.
71. Humphrey, W., A. Dalke, and K. Schulten, 1996. VMD: visual molecular dynamics. *J. Mol. Graph.* 14:33–38.
72. Tribello, G. A., M. Bonomi, D. Branduardi, C. Camilloni, and G. Bussi, 2014. PLUMED 2: New feathers for an old bird. *Comput. Phys. Commun.* 185:604–613.
73. Riccardi, E., A. Lervik, S. Roet, O. Aarøen, and T. S. van Erp, 2020. PyRETIS 2: an improbability drive for rare events. *Journal of computational chemistry* 41:370–377.
74. InfRETIS: Python libraries for running ∞ RETIS. <https://github.com/infretis/>, gitHub repository.
75. Vervust, W., D. T. Zhang, A. Ghysels, S. Roet, T. S. van Erp, and E. Riccardi, 2024. PyRETIS 3: Conquering rare and slow events without boundaries. *J. Comput. Chem.* .
76. Seeliger, M. A., B. Nagar, F. Frank, X. Cao, M. N. Henderson, and J. Kuriyan, 2007. c-Src binds to the cancer drug imatinib with an inactive Abl/c-Kit conformation and a distributed thermodynamic penalty. *Structure* 15:299–311.
77. Lyczek, A., B.-T. Berger, A. M. Rangwala, Y. Paung, J. Tom, H. Philipose, J. Guo, S. K. Albanese, M. B. Robers, S. Knapp, J. D. Chodera, and M. A. Seeliger, 2021. Mutation in Abl kinase with altered drug-binding kinetics indicates a novel mechanism of imatinib resistance. *Proc. Natl. Acad. Sci. U.S.A.* 118:e2111451118.
78. Agafonov, R. V., C. Wilson, R. Otten, V. Buosi, and D. Kern, 2014. Energetic dissection of Gleevec’s selectivity toward human tyrosine kinases. *Nat. Struct. Mol. Biol.* 21:848–853.
79. Narayan, B., N.-V. Buchete, and R. Elber, 2021. Computer simulations of the dissociation mechanism of Gleevec from Abl Kinase with milestoning. *J. Phys. Chem. B* 125:5706–5715.
80. Shekhar, M., Z. Smith, M. A. Seeliger, and P. Tiwary, 2022. Protein flexibility and dissociation pathway differentiation can explain onset of resistance mutations in kinases. *Angew. Chem. Int. Ed.* 61:e202200983.
81. van Erp, T. S., 2006. Efficiency analysis of reaction rate calculation methods using analytical models I: The two-dimensional sharp barrier. *J. Chem. Phys.* 125.
82. Allen, R. J., C. Valeriani, and P. R. Ten Wolde, 2009. Forward flux sampling for rare event simulations. *J. Phys.: Condens. Matter* 21:463102.
83. Frenkel, D., and B. Smit, 2023. Understanding molecular simulation: from algorithms to applications. Elsevier.
84. Huber, G. A., and S. Kim, 1996. Weighted-ensemble Brownian dynamics simulations for protein association reactions. *Biophysical journal* 70:97–110.
85. Cérou, F., A. Guyader, T. Lelièvre, and D. Pommier, 2011. A multiple replica approach to simulate reactive trajectories. *J. Chem. Phys.* 134.
86. van Heesch, T., P. G. Bolhuis, and J. Vreede, 2023. Decoding dissociation of sequence-specific protein–DNA complexes with non-equilibrium simulations. *Nucleic Acids Research* 51:12150–12160.
87. Weinan, E., W. Ren, and E. Vanden-Eijnden, 2002. String method for the study of rare events. *Physical Review B* 66:052301.
88. Maragliano, L., A. Fischer, E. Vanden-Eijnden, and G. Cicotti, 2006. String method in collective variables: Minimum free energy paths and isocommittor surfaces. *The Journal of chemical physics* 125.
89. Frassek, M., A. Arjun, and P. Bolhuis, 2021. An extended autoencoder model for reaction coordinate discovery in rare event molecular dynamics datasets. *The Journal of Chemical Physics* 155.
90. Belkacemi, Z., P. Gkeka, T. Lelièvre, and G. Stoltz, 2021. Chasing collective variables using autoencoders and biased trajectories. *Journal of chemical theory and computation* 18:59–78.

91. Fröhlking, T., L. Bonati, V. Rizzi, and F. L. Gervasio, 2024. Deep learning path-like collective variable for enhanced sampling molecular dynamics. *The Journal of Chemical Physics* 160.
92. Ayaz, P., A. Lyczek, Y. Paung, V. R. Mingione, R. E. Iacob, P. W. de Waal, J. R. Engen, M. A. Seeliger, Y. Shan, and D. E. Shaw, 2023. Structural mechanism of a drug-binding process involving a large conformational change of the protein target. *Nat. Commun.* 14:1885.
93. Rogal, J., and P. G. Bolhuis, 2008. Multiple state transition path sampling. *J. Chem. Phys.* 129.
94. Wu, H., and F. Noé, 2020. Variational approach for learning Markov processes from time series data. *Journal of Nonlinear Science* 30:23–66.
95. Vervust, W., 2024. Advanced Molecular Dynamics Simulation Techniques for Kinetic Analysis of Biological Systems. Doctoral dissertation, Ghent University, Faculty of Engineering and Architecture, Department of Electronics and Information Systems.
96. Falkner, S., A. Coretti, and C. Dellago, 2024. Enhanced Sampling of Configuration and Path Space in a Generalized Ensemble by Shooting Point Exchange. *Phys. Rev. Lett.* 132:128001.
97. Vervust, W., T. D. Zhang, E. Riccardi, T. S. van Erp, and A. Ghysels. ABL configurations. Dataset on Zenodo. <https://doi.org/10.5281/zenodo.14833469>.